

Halide vapor phase epitaxy of p-type Mg-doped GaN utilizing MgO

Kazuki Ohnishi^{1*}, Yuki Amano¹, Naoki Fujimoto², Shugo Nitta², Yoshio Honda², and Hiroshi Amano^{2,3,4}

¹ *Graduate School of Engineering, Nagoya University, Nagoya 464-8603, Japan*

² *Institute of Materials and Systems for Sustainability, Nagoya University, Nagoya 464-8601, Japan*

³ *Akasaki Research Center, Nagoya University, Nagoya 464-8603, Japan*

⁴ *Venture Business Laboratory, Nagoya University, Nagoya 464-8603, Japan*

E-mail: k.ohnishi@nagoya-u.jp

Halide vapor phase epitaxy (HVPE) of p-type GaN:Mg films was realized by using solid MgO as the Mg source. The Mg concentration was controlled by supplying HCl gas in a MgO source zone. Mg-related photoluminescence peaks were observed at around 3.3 and 2.9 eV. For a sample with a Mg concentration of $2.8 \times 10^{19} \text{ cm}^{-3}$, the Hall-effect measurement showed p-type conduction with a hole concentration and a hole mobility of $1.3 \times 10^{17} \text{ cm}^{-3}$ and $9.1 \text{ cm}^2\text{V}^{-1}\text{s}^{-1}$, respectively, at room temperature. The Mg acceptor level was $232 \pm 15 \text{ meV}$, which is in good agreement with the previous report.

GaN-based high-power devices are expected to be key products in an energy-saving and low-carbon-emitting society owing to their high breakdown electric field and high electron mobility^{1, 2}). To grow these device structures, the metalorganic vapor phase epitaxy (MOVPE) method has been commonly used. In this method, the incorporation of the carbon impurity in MOVPE-grown GaN films is unavoidable because metalorganics are used as group III precursors. Carbon impurity acts like not only an acceptor but also a donor³⁻⁷). To fabricate the high-performance vertical power devices, the reduction in a carbon impurity and the growth of thick GaN drift layers are required. To obtain a low carbon concentration, however, the growth rate of the MOVPE system must be as low as several $\mu\text{m/h}$, which is an obstacle for the growth of thick drift layers⁸).

Halide vapor phase epitaxy (HVPE) is well known as the method of fabricating GaN freestanding wafers⁹⁻¹¹). This method is also effective for fabricating GaN-based vertical power devices because it has a high growth rate of more than $100 \mu\text{m/h}$ and uses carbon-free sources enabling the growth of a thick GaN layer with a low carbon concentration. However, residual donors such as Si and O are incorporated in unintentionally doped (UID-) GaN owing to the use of the quartz reactor. Therefore, it is difficult to apply the HVPE method for the growth of high-purity GaN drift layers. Recently, Fujikura and co-workers have developed the quartz-free HVPE reactor and achieved reductions in residual Si and O concentrations to the order of 10^{14} cm^{-3} ^{12, 13}). For the growth of power-device structures such as a p-n diode, the fabrication of p-type GaN layers by HVPE is necessary. For the MOVPE system, p-type GaN has already been realized^{14, 15}). Additionally, p-type conduction in Mg-implanted GaN films was reported¹⁶). On the other hand, there are very few reports on fabricating p-type GaN films by HVPE¹⁷). **In the p-type GaN by HVPE, the acceptor level has not yet been clarified because the Hall effect measurement at room temperature was only reported as the evidence of p-type conduction¹⁷). Moreover, the Mg concentration has been controlled to the order of 10^{19} cm^{-3} by changing the growth rate¹⁷), which indicates that the Mg concentration cannot be controlled as the independent parameter. In case of vertical power metal-oxide-semiconductor field-effect transistor application, it is necessary to precisely control the Mg concentration in p-body layer¹⁸), although it is anticipated that the precise control of the Mg concentration in HVPE is difficult owing to the high equilibrium vapor pressure of Mg¹⁹). Thus, Mg metal is not favorable as a Mg precursor and a suitable Mg precursor must be investigated for fabricating p-type GaN layer by HVPE.**

MgO is an attractive material for the Mg doping source in the HVPE system. The melting

point of MgO is approximately 2800 °C and the vapor pressure of MgO is almost the same as that of quartz²⁰). Additionally, the reactivity between MgO and quartz is lower than that between Mg and quartz^{21, 22}). Therefore, MgO is thought to be stable in the HVPE reactor. Mg precursor can be supplied as magnesium chlorides formed by reacting MgO and HCl, which shows that the Mg concentration can be controlled merely by changing the HCl flow rate, thus we can precisely control the Mg concentration as the separate parameter from the growth rate. This technique can improve the controllability of Mg doping concentration without changing the growth rate. In this study, MgO was applied as a Mg doping source and the HVPE growth of Mg-doped GaN films was demonstrated. The optical and electrical properties of Mg-doped GaN films are also discussed.

The HVPE growth was performed in a horizontal HVPE system (TAIYO NIPPON SAN SO CORPORATION H-300) with three individual heat zones: two source zones and a growth zone. A schematic of the HVPE system for Mg doping is shown in Fig. 1. Source zones of a Ga melt and solid MgO were separated, and Ga, N, and Mg precursors were supplied to the growth zone heated at 1070 °C. In the case of Mg doping, a Mg precursor may be delivered as magnesium chlorides such as MgCl₂. These chlorides were formed by the reaction between solid MgO (MgO: 99.9%, Ca: 0.02%, Fe: 0.008%, and Al: 0.007%) and HCl gas at 900 °C. GaCl formed by the reaction between a Ga melt and HCl gas at 850 °C was used as a Ga precursor. NH₃ was used as a N precursor. The HCl flow rate in a Ga melt and the NH₃ flow rate were 40 sccm and 4 slm, respectively. N₂ and H₂ were used as the carrier gas and the H₂/(H₂ + N₂) ratio was 0.23. The growth rate was set to 25 – 30 μm/h. This growth rate was optimized for the growth of drift layers. The growth pressure was 1 atm. Approximately 25-μm-thick Mg-doped GaN films were grown by HVPE on 3-μm-thick UID-GaN/sapphire templates prepared by MOVPE. To investigate the effect of the Mg-doping concentration on the properties of Mg-doped GaN films, the HCl flow rate in MgO zone was varied from 0 to 10 sccm. Secondary ion mass spectroscopy (SIMS) was employed to investigate Mg, H, and O concentrations. Surface morphologies were observed using a Nomarski-type microscope (Nikon ECLIPSE LV150A). The optical property was evaluated by photoluminescence (PL) measurement at room temperature. In this PL measurement, a He-Cd laser with a wavelength of 325 nm was used as an excitation source. The electrical property was evaluated by van der Pauw Hall-effect measurement. This measurement was performed using the ToyoResitest8300 system under an AC magnetic field with an amplitude of 0.5 T. Before this measurement, samples were annealed at 700 °C in nitrogen ambient for 5 min to activate Mg. After annealing, Ni/Au (20 nm/200 nm) was deposited as a p-type electrode using an

electron beam evaporator. Samples were annealed at 525 °C in oxygen ambient for 5 min to obtain ohmic contacts.

The possibility of controlling the Mg concentration in Mg-doped GaN films by varying the HCl flow rate was investigated. The SIMS depth profile of the Mg concentration of as-grown GaN films with various HCl flow rates in a MgO zone is shown in Fig. 2(a). The Mg concentration of all samples was almost constant along the depth. From the SIMS measurement, averaged Mg, H, and O concentrations were calculated. The relationship between Mg, O, and H concentrations and the HCl flow rate in a MgO zone is shown in Fig. 2 (b). In all samples, the C concentration was lower than $2 \times 10^{15} \text{ cm}^{-3}$, which is the detection limit of SIMS. Also, the Si concentration of all samples was approximately $3 \times 10^{15} \text{ cm}^{-3}$, irrespective of the different HCl flow rate. **In the UID-GaN film when HCl flow rate was 0.0 sccm, the O concentration was $1.1 \times 10^{16} \text{ cm}^{-3}$. The Mg and H concentrations were lower than $6 \times 10^{14} \text{ cm}^{-3}$, and $3 \times 10^{16} \text{ cm}^{-3}$, respectively, which were both the detection limit.** By supplying HCl gas, the Mg concentration can be controlled to the order of $10^{19} - 10^{20} \text{ cm}^{-3}$. This result indicates that the Mg precursor can be magnesium chlorides such as MgCl_2 . **The order of the O concentration within the HCl flow rate was $10^{16} - 10^{18} \text{ cm}^{-3}$** , which was one to three orders of magnitude lower than that of the Mg concentration. The O concentration in Mg-doped GaN films was also increased by increasing HCl flow. Thus, the incorporated oxygen comes from MgO. To clarify the reaction among MgO, HCl, and N_2 , the theoretical approach such as thermodynamic calculation²³⁾ is important. Further investigation of this reaction will be reported elsewhere. The H concentration was of the same order as the Mg concentration. This behavior shows that Mg is incorporated in GaN films as a complex with H²⁴⁾. On the other hand, Usikov *et al.* suggested that the H concentration in a Mg-doped GaN film was approximately one order of magnitude lower than the Mg concentration owing to the use of inert gas as the carrier gas¹⁷⁾. In our HVPE growth ambient, the H_2 and N_2 mixture gas was used as the carrier gas. H_2 gas may enhance the formation of Mg – H complexes and the H concentration was larger than that described in Ref. 17.

In all samples, mirrorlike surfaces were obtained. The effect of Mg doping on the macroscopic surface morphology is shown in Fig. 3. This figure shows Nomarski-type microscopy images of Mg-doped GaN films with various Mg concentrations. With increasing Mg concentration, some hillocks were observed. However, there were smooth enough for the growth of device structures.

Then, the optical and electrical properties of Mg-doped GaN films grown by HVPE were investigated. Figure 4 shows the room-temperature PL spectra of UID-GaN film and Mg-

doped GaN films with various Mg concentrations. In the typical UID-GaN film grown by our HVPE system, the near-band-edge (NBE) emission was clearly observed at 3.4 eV. From the sample with the Mg concentration of $1.5 \times 10^{19} \text{ cm}^{-3}$, two emission peaks were observed: NBE emission at 3.4 eV and the ultraviolet luminescence (UVL) at around 3.3 eV. In the sample with the Mg concentration of $4.4 \times 10^{19} \text{ cm}^{-3}$, the PL intensity of NBE emission was lower than that in a sample with the Mg concentration of $1.5 \times 10^{19} \text{ cm}^{-3}$. The blue luminescence (BL) at around 2.9 eV was also observed. By increasing Mg concentration, the dominant PL intensity was changed from the NBE emission to the BL. These PL spectra showed the same tendency as those of Mg-doped GaN films grown by MOVPE²⁵. In the case of the Mg-doped GaN films grown by MOVPE, the UVL and BL are due to a free electron or a shallow donor to a Mg acceptor substituted into a Ga site (Mg_{Ga}) and the recombination of a deep donor to a Mg_{Ga} pair (DAP), respectively²⁶. Additionally, the dominant PL intensity changed from 3.4 to 2.8 eV with increasing Mg concentration²⁵. Therefore, The UVL and BL of samples by HVPE are both related to the emission from the Mg acceptor. When the Mg concentration was increased to 6.8×10^{19} and $9.0 \times 10^{19} \text{ cm}^{-3}$, broad emission peaks were observed at around 2.5 and 3.2 eV. For the Mg-doped and Mg-implanted GaN films, the emission peak at around 2.4 eV is attributed to nitrogen vacancies²⁷. Additionally, the formation of some donors is easy owing to the self-compensation effect in highly Mg-doped GaN films^{25, 28}. Moreover, O concentrations increased to 10^{18} cm^{-3} . Thus, it is considered that broad emission peaks are attributed to some donors owing to the self-compensation effect and the O incorporation.

The Hall-effect measurement was performed to determine the conduction type, hole concentration, and hole mobility. In this study, the hole concentration and hole mobility were calculated assuming a Hall factor of 1. An approximately 30- μm -thick Mg-doped GaN film with a Mg concentration of $2.8 \times 10^{19} \text{ cm}^{-3}$ grown under the same HVPE growth condition showed p-type conduction. The hole concentration and mobility at room temperature were $1.3 \times 10^{17} \text{ cm}^{-3}$ and $9.1 \text{ cm}^2\text{V}^{-1}\text{s}^{-1}$, respectively. Figure 5(a) shows the temperature dependence of the hole concentration for the sample. To estimate the acceptor concentration N_A , the donor concentration N_D , and the ionization energy E_A , a fitting analysis for the hole concentration was performed. This analysis was based on the charge neutrality condition and carrier statistics. The effective density of states in the valence band at 300 K of $7.3 \times 10^{19} \text{ cm}^{-3}$ was taken from Ref. 29. Before fitting, we considered the dependence of E_A , which decreases with increasing N_A owing to the Coulomb potential of ionized impurities³⁰. E_A of the acceptor is expressed as^{29, 31-33}

$$E_A = E_{A0} - f(p + N_D)^{1/3} \quad (1)$$

$$f = \Gamma(2/3) \left(\frac{4\pi}{3}\right)^{1/3} \frac{q^2}{4\pi\epsilon_s}, \quad (2)$$

where E_{A0} is the acceptor level at a sufficiently low acceptor concentration, $\epsilon_s = 9.5\epsilon_0$ is the dielectric constant for GaN³⁴), q is the elementary charge, and ϵ_0 is the dielectric constant of vacuum. By considering Eqs. (1) and (2), the fitting analysis was performed. The Mg concentration and the calculated values are presented in Table 1. N_A is slightly higher than the Mg concentration. In the case of p-type GaN films grown by MOVPE, N_A is close to the Mg concentration or higher^{29, 35}). Horita *et al.* suggested this to be due to the error in **the effective density of states in the valence band** at 300 K or the difference in Hall factor from unity²⁹). From the SIMS measurement, the Si and O concentrations were 2.4×10^{15} and $4.3 \times 10^{16} \text{ cm}^{-3}$, respectively. N_D/N_A was approximately 9%. The sum of Si and O concentrations was approximately 1.5% of N_D . It is considered that not only the residual Si and O but also native defects are the origin of donors. Furthermore, the calculated E_{A0} , which was $232 \pm 15 \text{ meV}$, was in good agreement with the reported value of $245 \pm 25 \text{ meV}$ ^{29, 36}). Figure 5(b) shows the temperature dependence of the hole mobility. Above 200 K, the hole mobility decreased with increasing temperature, which suggests that phonon scattering is dominant.

In conclusion, the HVPE growth of Mg-doped GaN films and the p-type conduction were achieved by using solid MgO as a Mg doping source. The Mg concentration of $10^{19} - 10^{20} \text{ cm}^{-3}$ was controlled by varying the HCl flow rate in the MgO source zone. This result suggests that MgO can react with HCl, whereby Mg is supplied into the GaN growth zone as magnesium chlorides. From PL measurements, the Mg-related emissions were observed at 3.3 and 2.9 eV, and the emission peak at 2.9 eV became more significant with increasing Mg concentration. The Hall-effect measurement showed p-type conduction in the sample with a Mg concentration of $2.8 \times 10^{19} \text{ cm}^{-3}$ at room temperature. The hole concentration and mobility were $1.3 \times 10^{17} \text{ cm}^{-3}$ and $9.1 \text{ cm}^2\text{V}^{-1}\text{s}^{-1}$, respectively. The acceptor level was $232 \pm 15 \text{ meV}$. According to the results, solid MgO is promising for Mg doping in the method of fabricating p-type GaN films by HVPE.

Acknowledgments

This research is supported by the MEXT “Program for research and development of next-generation semiconductor to realize energy-saving society” Program Grant Number JPJ005357 and a project commissioned by the New Energy and Industrial Technology

Development Organization (NEDO).

References

- 1) T. Kachi, *Jpn. J. Appl. Phys.* **53**, 100210 (2014).
- 2) T. Oka, *Jpn. J. Appl. Phys.* **58**, SB0805 (2019).
- 3) J. L. Lyons, A. Janotti, and C. G. Van de Walle, *Appl. Phys. Lett.* **97**, 152108 (2010).
- 4) D. O. Demochenko, I. C. Diallo, and M. A. Reshchikov, *Phys. Rev. Lett.* **110**, 087404 (2013).
- 5) J. L. Lyons, A. Janotti, and C. G. Van de Walle, *Phys. Rev. B* **89**, 035204 (2014).
- 6) N. Sawada, T. Narita, M. Kanechika, T. Uesugi, T. Kachi, M. Horita, T. Kimoto, and J. Suda, *Appl. Phys. Express* **11**, 041001 (2018).
- 7) T. Narita, K. Tomita, Y. Tokuda, T. Kogiso, M. Horita, and T. Kachi, *J. Appl. Phys.* **124**, 215701 (2018).
- 8) G. Piao, K. Ikenaga, Y. Yano, H. Tokunaga, A. Mishima, Y. Ban, T. Tabuchi, K. Matsumoto, *J. Cryst. Growth* **456**, 137 (2016).
- 9) A. Usui, H. Sanakawa, and A. A. Yamaguchi, *Jpn. J. Appl. Phys.* **36**, L899 (1997).
- 10) K. Motoki, T. Okahisa, N. Matsumoto, M. Matsushita, H. Kimura, H. Kasai, K. Takemoto, K. Umetsu, T. Hirano, M. Nakayama, S. Nakahata, M. Ueno, D. Hara, Y. Kumagai, A. Koukitu, and H. Seki, *Jpn. J. Appl. Phys.* **40**, L140 (2001).
- 11) Y. Oshima, T. Eri, M. Shibata, H. Sunakawa, K. Kobayashi, T. Ichihashi, and A. Usui, *Jpn. J. Appl. Phys.* **42**, L1 (2003).
- 12) H. Fujikura, T. Konno, T. Yoshida, and F. Horikiri, *Jpn. J. Appl. Phys.* **56**, 085503 (2017).
- 13) K. Kanegae, H. Fujikura, Y. Otoki, T. Konno, T. Yoshida, M. Horita, T. Kimoto, and J. Suda, *Appl. Phys. Lett.* **115**, 012103 (2019).
- 14) H. Amano, M. Kito, K. Hiramatsu, and I. Akasaki, *Jpn. J. Appl. Phys.* **28**, L2112 (1989).
- 15) S. Nakamura, T. Mukai, M. Senoh, and N. Iwasa, *Jpn. J. Appl. Phys.* **31**, L139 (1992).
- 16) H. Sakurai, M. Omori, S. Yamada, Y. Furukawa, H. Suzuki, T. Narita, K. Kataoka, M. Horita, M. Bockowski, J. Suda, and T. Kachi, *Appl. Phys. Lett.* **115**, 142101 (2019).
- 17) A. Usikov, O. Kovalenkov, V. Soukhoveev, V. Ivantsov, A. Syrkin, V. Dmitriev, A. Yu. Nikiforov, S. G. Sundaresan, S. J. Jeliazkov, and A. V. Davydov, *Phys. Status Solidi C* **5**, 1829 (2008).
- 18) S. Takashima, K. Ueno, H. Matsuyama, T. Inamoto, M. Edo, T. Takahashi, M. Shimizu, and K. Nakagawa, *Appl. Phys. Express* **10**, 121004 (2017).
- 19) C. B. Alcock, V. P. Itkin, and M. K. Horrigan, *Can. Metall. Quart.* **23**, 309 (1984).

- 20) T. Sata, *J. Mineral. Soc. Jpn.* **16**, 137 (1983).
- 21) I. Gutman, L. Klinger, I. Gotman, and M. Shapiro, *Scripta Mater.* **45**, 363 (2001).
- 22) G. W. Brindley and R. Hayami, *Phil. Mag.* **12**, 505 (1965).
- 23) A. Koukitu, S. Hama, T. Taki, and H. Seki, *Jpn. J. Appl. Phys.* **37**, 762 (1998).
- 24) J. Neugebauer and C. G. Van de Walle, *Phys. Rev. Lett.* **75**, 4452 (1995).
- 25) H. Obloh, K. H. Bachem, U. Kaufmann, M. Kunzer, M. Meir, A. Ramakrishnan, and P. Schlotter, *J. Cryst. Growth* **195**, 270 (1998).
- 26) M. A. Reshchikov and H. Morkoç, *J. Appl. Phys.* **97**, 061301 (2005).
- 27) M. A. Reshchikov, D. O. Demchenko, J. D. McNamara, S. Fernández-Garrido, and R. Calarco, *Phys. Rev. B* **90**, 035207 (2014).
- 28) C. G. Van de Walle and J. Neugebauer, *J. Appl. Phys.* **95**, 3851 (2004).
- 29) M. Horita, S. Takashima, R. Tanaka, H. Matsuyama, K. Ueno, M. Edo, T. Takahashi, M. Shimizu, and J. Suda, *Jpn. J. Appl. Phys.* **56**, 031001 (2017).
- 30) B. Šantić, *Semicond. Sci. Technol.* **21**, 1484 (2006).
- 31) G. L. Pearson and J. Bardeen, *Phys. Rev.* **75**, 865 (1949).
- 32) P. P. Debye and E. M. Conwell, *Phys. Rev.* **93**, 693 (1954).
- 33) W. Götz, R. S. Kern, C. H. Chen, H. Liu, D. A. Steigerwald, and R. M. Fletcher, *Mater. Sci. Eng. B* **59**, 211 (1999).
- 34) K. Karch, J.-M. Wagner, and F. Bechstedt, *Phys. Rev. B* **57**, 7043 (1998).
- 35) T. Narita, K. Tomita, K. Kataoka, Y. Tokuda, T. Kogiso, H. Yoshida, N. Ikarashi, K. Iwata, M. Nagao, N. Sawada, M. Horita, J. Suda, and T. Kachi, *Jpn. J. Appl. Phys.* **59**, SA0804 (2020).
- 36) S. Brochen, J. Brault, S. Chenot, A. Dussaigne, M. Leroux, and B. Damilano, *Appl. Phys. Lett.* **103**, 032102 (2013).

Table I.

Mg concentration (cm^{-3})	N_{A} (cm^{-3})	N_{D} (cm^{-3})	E_{A0} (meV)
2.8×10^{19}	3.4×10^{19}	3.0×10^{18}	232 ± 15

Figure Captions

Table 1. Acceptor concentration, donor concentration, and ionization energy obtained by Hall-effect measurement of p-type GaN with Mg concentration of $2.8 \times 10^{19} \text{ cm}^{-3}$.

Fig. 1. Schematic of the HVPE system for the growth of Mg-doped GaN films using MgO.

Fig. 2. (a) SIMS depth profile of Mg concentration for Mg-doped GaN films with various HCl flow rates in the MgO zone and (b) Mg, H, and O concentrations as a function of HCl flow rate.

Fig. 3. Nomarski-type microscopy images of samples with various Mg concentrations.

Fig. 4. Room-temperature PL spectra of UID-GaN film and Mg-doped GaN films with various Mg concentrations.

Fig. 5. Temperature dependence of (a) hole concentration and (b) hole mobility of the sample with Mg concentration of $2.8 \times 10^{19} \text{ cm}^{-3}$.

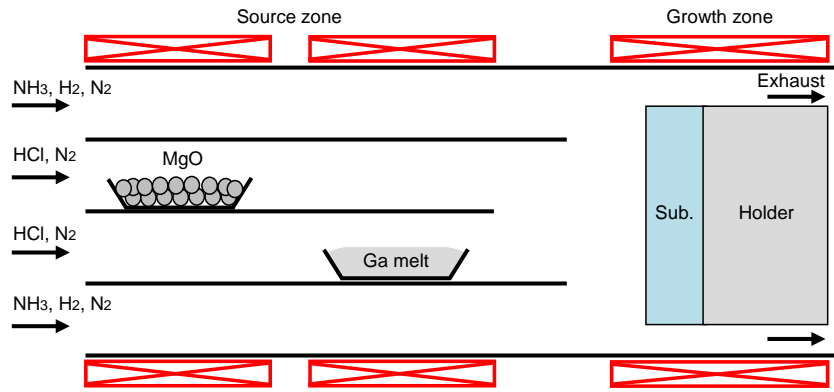
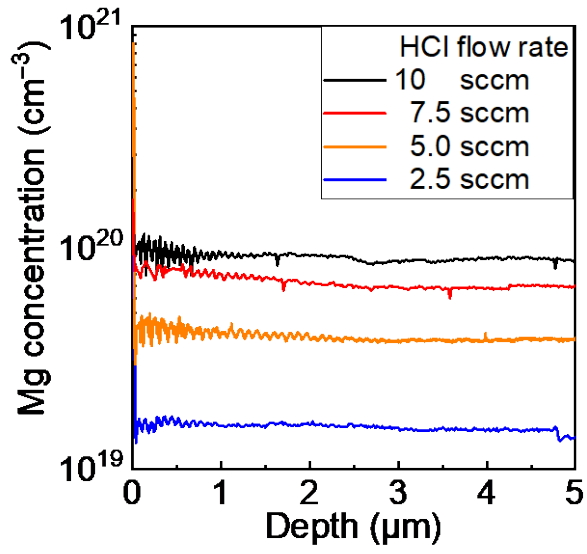
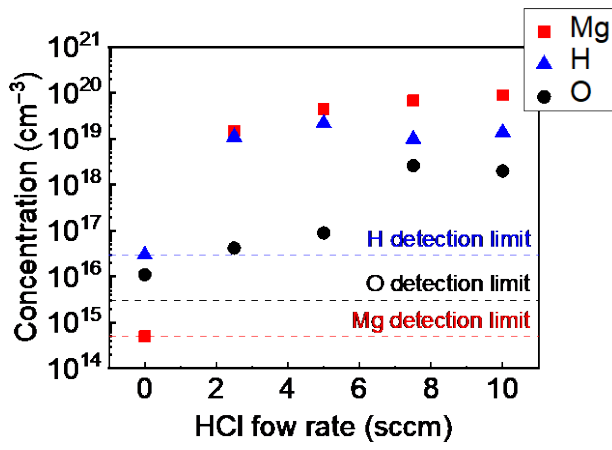


Fig. 1.



(a)



(b)

Fig. 2.

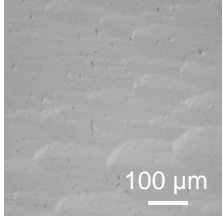
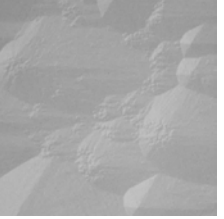
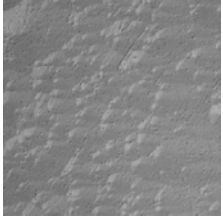
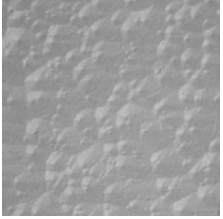
Mg concentration (cm^{-3})	1.5×10^{19}	4.4×10^{19}	6.8×10^{19}	9.0×10^{19}
Nomarski-type microscopy image				

Fig. 3.

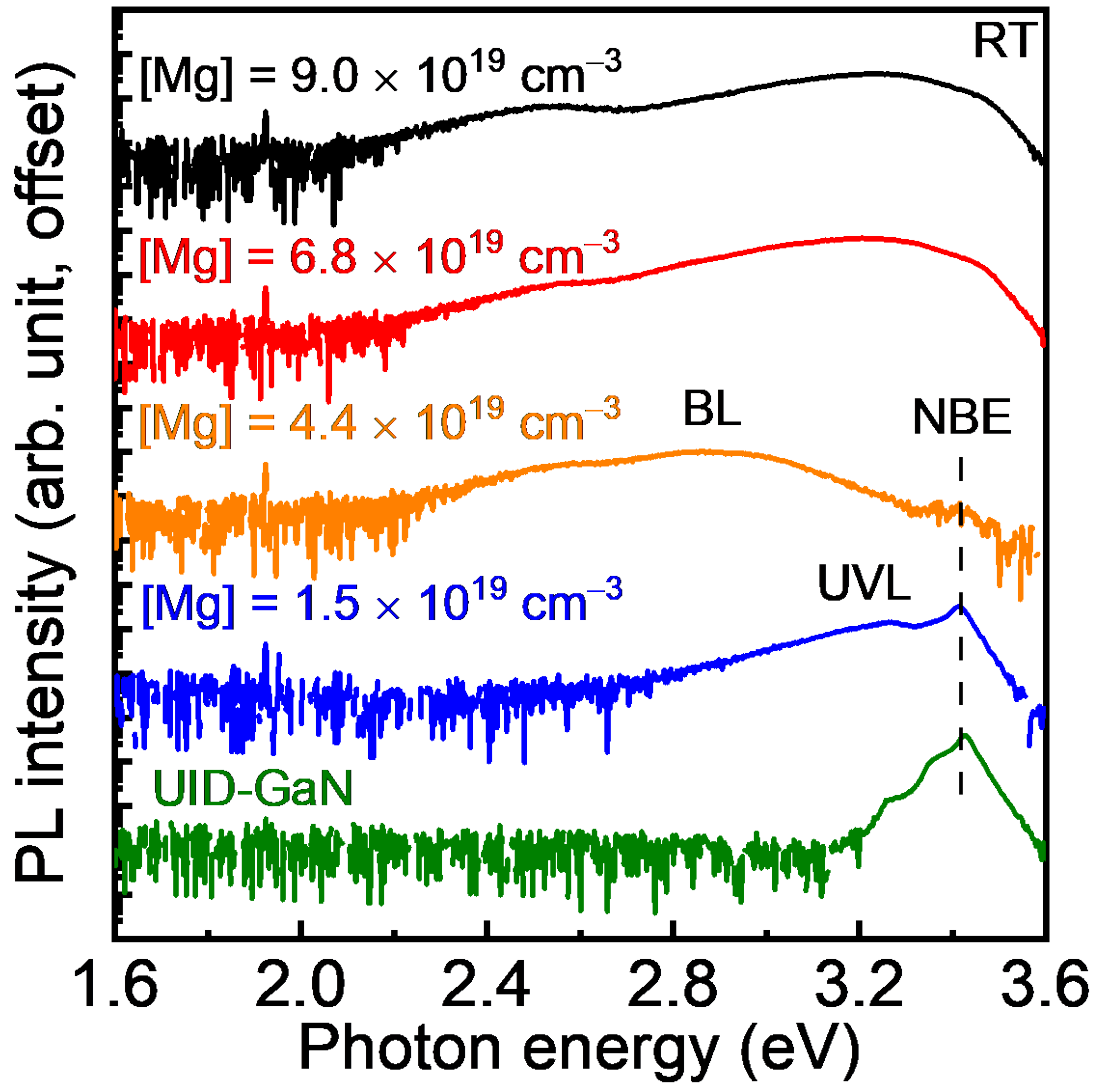
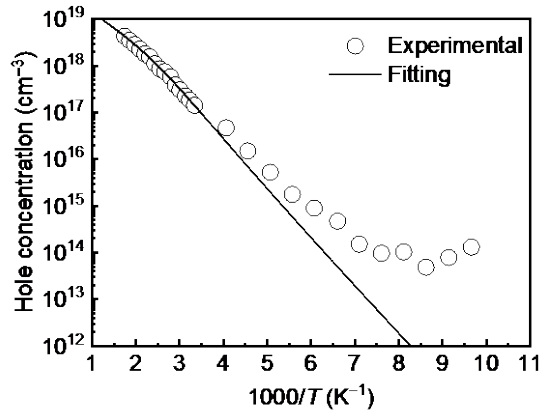
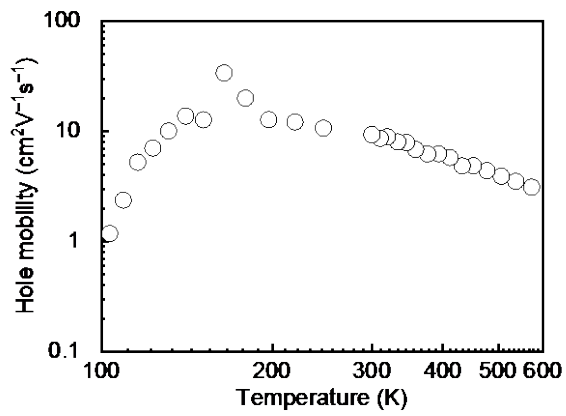


Fig.4.



(a)



(b)

Fig. 5.